Eur. Phys. J. AP **8**, 215–224 (1999)

THE EUROPEAN PHYSICAL JOURNAL APPLIED PHYSICS

Annealing and thickness effects on some electrical and optical properties of Sb:SnO_2 films

E.Kh. Shokr[a], M.M. Wakkad, H.A. Abd El-Ghanny, and H.M. Ali

Physics Department, Faculty of Science, Sohag, Egypt

Received: 13 January 1999 / Revised: 12 August 1999 / Accepted: 7 October 1999

Abstract. Effects of annealing and film thickness on the electrical and optical properties of Sb:SnO_2 films deposited by electron beam from bulk samples prepared using sintering technique have been investigated. A compromise between low resistivity and high transparency of the film has been studied using the factor of merit. This factor, which has been found maximum for film 100 nm thick annealed at 550 °C for 15 min, seemed to be enhanced with increasing annealing time and/or film thickness confirming the simultaneous improvements of transparency and conductance with the latters. Other optical and electrical parameters such as refractive index, width of energy gap, density of localized states, concentration and mobility of carriers and Seebeck coefficient have been studied also, discussed and correlated to the microstructure changes with annealing and film thickness.

PACS. 73.61.-r Electrical properties of specific thin films and layer structures (multilayers, superlattices, quantum wells, wires, and dots) – 78.66.-w Optical properties of specific thin films, surfaces, and low-dimensional structures

1 Introduction

Semiconductor oxides in general, and undoped or doped tin oxide in particular, have attracted much interest for many applications [1–6]. The main objective of studies on thin SnO_2-based films has been the preparation of films with high transparency and high electrical conductivity. Therefore, intensive studies [7–12] on Sb-doped SnO_2 films regarding the changes in dopant concentration, heat treatment, temperature and type of substrate, precoating and film thickness have mainly aimed to improve simultaneously their transmittance and resistivity. In addition, different methods of preparation and deposition techniques [13–17] have been employed to obtain conductive transparent SnO_2-based films, since the properties of films depend on the condition of preparation and vary considerably from one technique to another.

However, for Sb:SnO_2 films deposited by spray pyrolysis it has been confirmed by Kojima *et al.* [7–10] that when the amorphinity increases in the film structure, which reduces its electrical conductivity, its transparency improves; and *vice versa*. So, a compromise between a low resistivity and a high transmittance of light mostly in the visible range, is required to reach. For this purpose, the so-called factor of merit, which represents the quality of the Sb:SnO_2 material as regards to the compromise to found between optical transmission and electrical resistivity [11, 18], can be used. This factor has been found maximum for Sb doping around 7% for Sb:SnO_2 films obtained by sol-gel method [11], and at Sb/Sn = 0.1 for films evaporated by electron beam [19].

In the present study, we have used electron beam evaporation to deposit thin Sb:SnO_2 films with Sb/Sn = 0.1 from their bulky form prepared using sintering method after mixing and pressing appropriate amounts of SnO_2 and Sb powders. Structure of films elaborated by this method seems to be composed of some crystalline phases, which are embedded in a glassy matrix. Besides, it was shown that, the glassy matrix, which is mainly raised due to the incorporated antimony that acts as a glass network former [20], is slightly changed in the film structure with annealing and film thickness changes. On the other hand, the intensities of crystalline phases were found to be enhanced with both annealing and film thickness. Thus, the film conductivity and transmittance can be improved due to these changes in crystalline and glassy phases of the structure caused by annealing and film thickness.

In addition, the probably existed oxygen vacancies in the film structure may lead to simultaneous improvements of its transparency and conductance. From one side, the deficiency of oxygen in the structure, which results in an asymmetrical atmosphere around Sb^{3+} and Sb^{5+} ions [9,21], makes it difficult for electron exchange between the two states Sb^{3+} and Sb^{5+} of antimony oxides and consequently for energy absorption to take place [9,21,22]. This leads to improve the film transparency. From the other side, these oxygen vacancies that make the structure to be deviated from stoichiometry and act as electron donors [20,23], contribute to the electrical conductivity.

[a] e-mail: eshokr@yahoo.com

Thus, the electrical and optical properties of Sb:SnO_2 films with such structural features deserve a comprehensive investigation. Films $\sim$ 100 nm thick, which is the employed thickness for many applications [24–26], have been mainly used in the present investigation.

2 Experimental technique

Appropriate portions of highly pure (4N) Sb and (5N) SnO_2 powders have been grinded separately and sieved. Mixture of Sb:SnO_2 with Sb/Sn = 0.1 (in atomic weight) has been prepared using suitable ratios of Sb and SnO_2 having almost equal particle sizes ($\sim$ 77μm). To insure complete mixing, this mixture has been grinded for at least three hours. Then, it has been made in a tablet form by using a cold pressing technique. These tablets have been, firstly, heat -treated at 600 °C for 5 h in air in order to avoid the migration of Sb atoms to the surface that can be observed as $T >$ 600–700 °C [8,27,28]. Besides, we think that the heat treatment at 600 °C can result in a highly diffusion rate of Sb atoms (melting point of Sb $\approx$ 631 °C) leading to an improvement of the material homogeneity and, may be, a production of, especially, Sb-O bonds. Then, sintering, which is usually carried out in the temperature range $\frac{T_{\rm M}}{2} \leq {\rm T} \lesssim T_{\rm M}$ where $T_{\rm M}$ is the melting point of the material to be sintered, has been performed for the present mixture at 900 °C for 4 h. Sintering process is oftenly accompanied by grain growth and, may be, crystallization.

Thin films of the prepared Sb:SnO_2 tablet were deposited onto ultrasonically cleaned corning glass substrates by electron beam evaporation at 2×10^{-5} torr using Edwards high vacuum coating unit model E306A. The provided rotatilt workholder drive system with angular control facilities permits the film substrates to be in the face of the material source and rotated with a controlled speed during deposition. This may insure a highly degree of film uniformity. The film thickness ($\sim$ 100–200 nm) and the deposition rate ($\sim$ 10 nm/min) were controlled by means of a calibrated digital film thickness monitor model TM200 Maxtek. The interference fringes appeared in the transmission spectra for some thicker films of SnO_2 (900-1200 nm thick) elaborated by the same present argument, were employed to determine their actual thicknesses (with an accuracy of better than 1%) using a procedure devised by Manifacier *et al.* [29]. Comparing these values of thickness with their corresponding values obtained by the thickness monitor, the latter could be calibrated. Silver paste electrodes with separation of 2 mm were used.

Investigations of the microstructure were carried out using an X-ray diffractometer (Philips model PW 1710) and scanning electron microscope (Jeol JSM-5300).

The film resistivity was measured in the 80–475 K temperature range by means of a variable temperature liquid nitrogen cryostat (Oxford DN-1710) combined with a programmable temperature controller (Oxford ITC4) and a digital Keithley 614 electrometer.

The thermal emf resulted due to the temperature gradient between the film electrodes was measured using a (Keithley 614) electrometer. The electrodes' temperature difference ΔT was monitored using a differential copper-constantan thermocouple.

A Jasco model V-570 (UV-Visible-NIR) double beam Spectrophotometer (with photometric accuracy of $\pm$ 0.002–0.004 Abs. and $\pm$ 0.3% Trans.) was employed to record the transmission T and reflection R spectra over the wavelength range from 200 to 2500 nm at normal incidence. In the region of interband transition having strong absorption, both the absorption coefficient α_0 and the refractive index n could be estimated using the following approximate relations [30,31] respectively,

$$\alpha_0 = \frac{1}{t}\ln\left[\frac{(1-R)^2}{T}\right] \quad \text{and} \tag{1}$$

$$n = \frac{1+R}{1-R} \pm \left[\left(\frac{R+1}{R-1}\right)^2 - (1+k^2)\right]^{1/2} \tag{2}$$

where t is the thickness of the film and $k = \alpha_0\lambda/4\pi$ is the extinction coefficient. Reasonable values for n have been obtained using the plus sign of equation (2). However, in the NIR spectral region, where the films are very transparent and the interference fringes are absent, values of α_0 and n could not be calculated.

3 Results

The temperature dependence of the electrical conductivity $\sigma(T)$ for as-deposited and annealed Sb:SnO_2 films in the range of T from 80 to about 475 K is shown in Figure 1. The plot suggests that there are two types of conduction channels that contribute to the conductivity. While σ is nearly insensitive to temperature in the low wide range of the latter, it seems to be thermally activated in the high range of T and can be described by the relation $\sigma = \sigma_0 \exp(-\Delta E/KT)$, where ΔE is the corresponding activation energy and σ_o is the pre-exponential factor. Values of ΔE were calculated and listed in Table 1 as a function of annealing temperature $T_{\rm an}$. However, the non-activated behaviour exhibited by $\sigma(T)$ in the low temperature region confirms that, $\sigma(T)$ is characterized by hopping conduction between the localized states. Therefore, the conductivity data in the low temperature regions can be analyzed on the basis of the following Mott's formula for variable-range hopping [32],

$$\sigma(T) = \frac{\sigma_o'}{\sqrt{T}}\exp\left[-\left(\frac{T_o}{T}\right)^{1/4}\right]$$

where σ_o' is the pre-exponential factor and $T_0 = 16\alpha^3/KN(E_{\rm f})$, where $N(E_{\rm f})$ is the density of localized states, α describes the spatial extent of the localized wave function and K is the Boltzmann's constant. Assuming that $\alpha = 0.124$ Å^{-1} [33], values of $N(E_{\rm f})$ for both

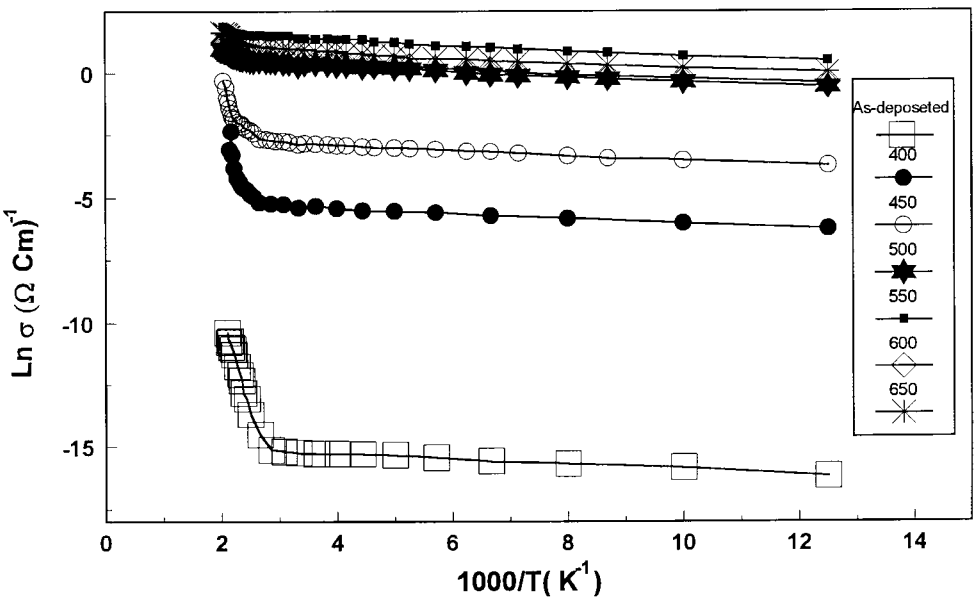

Fig. 1. Ln σ *versus* $1000/T$ plots for as deposited and annealed Sb:SnO_2 films at different temperatures for 15 min, $t = 100$ nm.

as-deposited and annealed films were estimated and summarized in Table 1. It is seen that, values obtained for $N(E_f)$ are relatively high. Besides, the uncertainties in these values are significantly high especially in the case of as-deposited film. Similar high uncertainties in some electrical and optical parameters of Sb:SnO_2 films such as mobility, activation energy, number of carriers and band gap width have been found formerly [11,19]. However, it is clear that the increase of annealing temperature results in a diminution of the density of the localized states.

Figure 2 shows that the room temperature (300 K) resistivity ρ_{RT} of Sb:SnO_2 films decreases gradually with elevating the temperature of annealing reaching its minimum value (0.324 Ωcm) at 550 °C, then it increases slightly with further elevation of T_{an}. Besides, more decrease in ρ_{RT} can be achieved with either elongation of annealing time at $T_{an} = 550$ °C or increase of thickness of films annealed for $t_{an} = 180$ min at $T_{an} = 550$ °C as shown in Table 2.

Data of thermoelectric power emf_{th} resulting due to the temperature difference ΔT between the film electrodes was measured for annealed Sb:SnO_2 films at room temperature. However, we were not able to obtain reliable thermopower data for as-deposited film due to its high resistance ($> 10^9$ Ω) which makes some residual voltage to be superimposed over thermal emf. Figure 2 shows the variation of Seebeck coefficient S, ($S = emf_{th} / \Delta T$), with annealing temperature T_{an}. It is clear that S has a negative sign, small values and generally decreases as T_{an} increases. Besides, as shown in Table 2, the increase of either annealing time or thickness of annealed films leads to the increase in the value of $|S|$.

The effects of annealing temperature on the transmittance and reflectance of Sb:SnO_2 films with 100 nm thick, are as shown in Figure 3. As seen from this figure, all films have absorption edge at about 300 nm. Maximum transmittance, which is clearly seen at 628 nm for as-deposited film, shifts towards lower values of λ to be around solar maximum wavelength ($\lambda = 500$ nm) as the temperature of annealing increases. Besides, Figure 4 shows that, the average value of the transmittance (T_m) in the (270-780 nm) spectral range increases from 0.43 for as-deposited film to 0.70 with elevating T_{an} to 600 °C. However elevation of annealing temperature over 600 °C is associated with a decrease in film transmittance. On the other hand, as shown in Table 2 higher values of T_m, which are larger than 0.8, have been achieved with annealing films at 550 °C for longer periods. However, increasing the film thickness makes T_m to be inhibited. In the NIR spectral region, while the reflection decreases, the transmission increases with increasing λ confirming the high transparency of the present films in the NIR as well in the visible spectral regions (Fig. 3).

Analysis of the results indicated that, the rapid change occurred in $\propto_o$ near the absorption edge can be interpreted as an optical transition [30]. Jousse [34] and Kojima *et al.* [9] have deduced the gap width E_g of such transition from the intercepts of the linear portions of the $(\alpha_o h\nu)^{1/2}$ *versus* $h\nu$ plots near the absorption edge to $(\alpha_o h\nu)^{1/2} = 0$, a matter that characterizes an allowed indirect transition. Values of E_g (with an uncertainty of ± 0.4) of the present films determined using the same argument are represented in Figure 4 as a function of T_{an}. As seen from this figure, E_g abruptly increases from about 2.4 eV for as-deposited film to ∼ 3.6 eV for film annealed at 400 °C. With elevation of T_{an} over 400 °C, E_g increases slightly tending to a saturation value of about 3.8 eV. This increase in E_g with T_{an} is expected since the density of localized states is reduced with the latter.

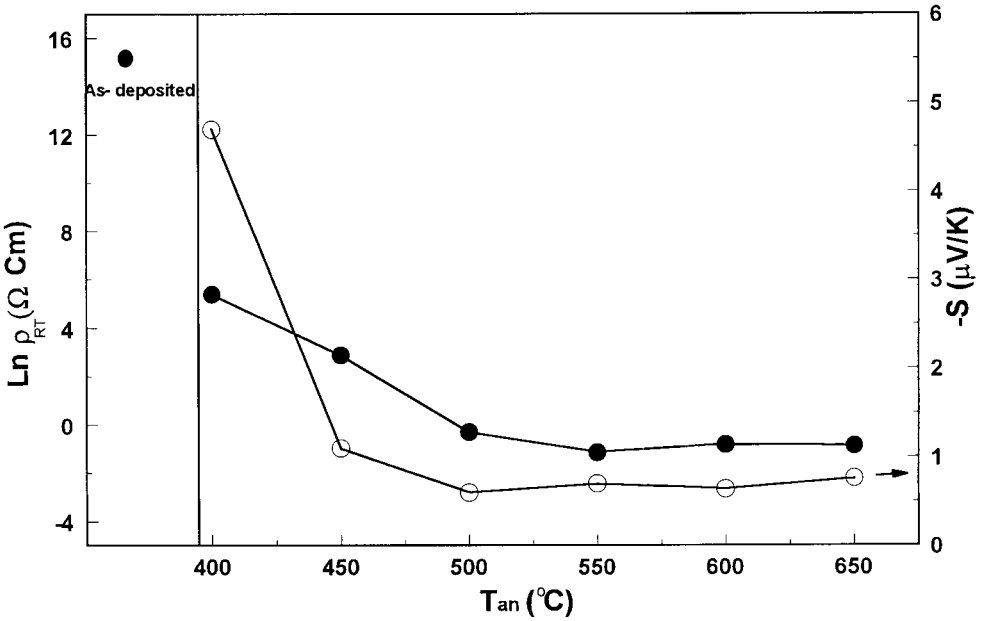

Fig. 2. Variations of the resistivity and Seebeck coefficient measured at room temperature for Sb:SnO_2 films annealed at different temperatures for 15 min, $t = 100$ nm.

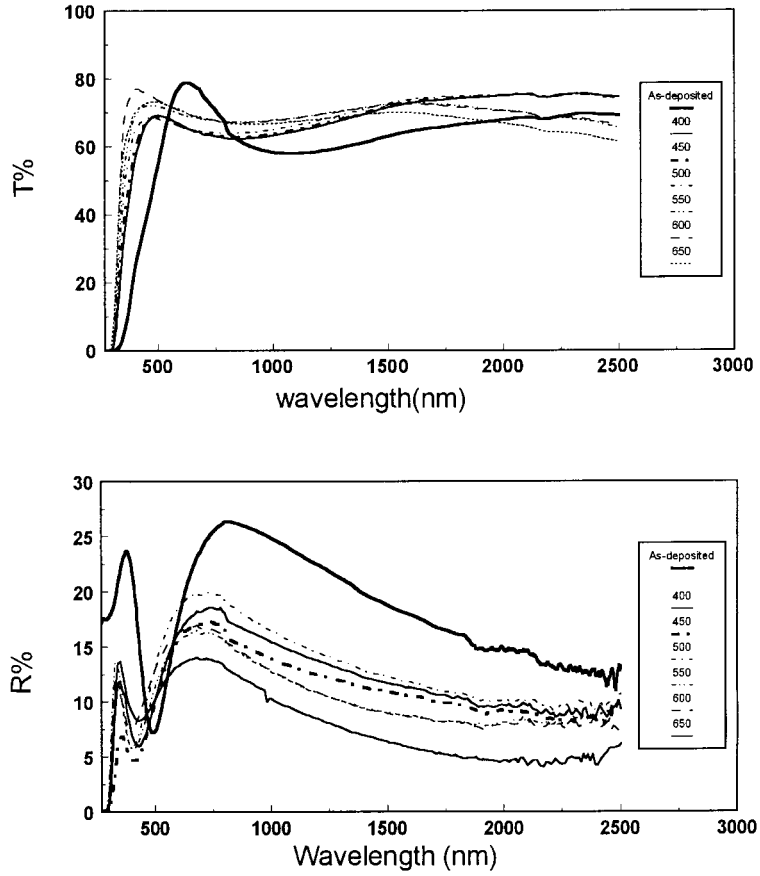

Fig. 3. Spectral variations of the transmittance T and reflectance R for either as-deposited or annealed Sb:SnO_2 films at different temperatures for 15 min, $t = 100$ nm.

Table 1. Effect of annealing temperature on some optical and electrical parameters. $t = 100$ nm, $t_{an} = 15$ min. $\bar{n}$ is the mean value of the refractive index in the 325-440 nm spectral range.

Annealing condition	ΔE (eV)	$N(E_f)$ (10^{21} $eV^{-1}cm^{-3}$)	N ($10^{20}cm^{-3}$)	μ ($cm^2V^{-1}s^{-1}$)	$\bar{n}$
As-deposited	0.35-0.97	1.67-5.63	0.59-4.45	(3.38-25.50) × 10−9	1.98
T_{an}(°C) = 400	0.38-0.40	1.95-2.69	2.01-2.77	(1.02-1.43) × 10^{-4}	2.03
450	0.30-0.32	1.85-2.66	1.92-2.79	(1.25-1.85) × 10^{-3}	1.96
500	0.078-0.082	1.86-2.52	1.96-2.66	(3.10-4.30) × 10^{-2}	2.03
550	0.059-0.061	1.67-2.31	1.85-2.55	(7.60-10.70) × 10^{-2}	2.16
600	0.098-0.102	1.65-2.25	1.84-2.50	(5.60-7.80) × 10^{-2}	2.16
650	0.088-0.092	1.53-2.17	1.75-2.49	(5.90-8.60) × 10^{-2}	2.18

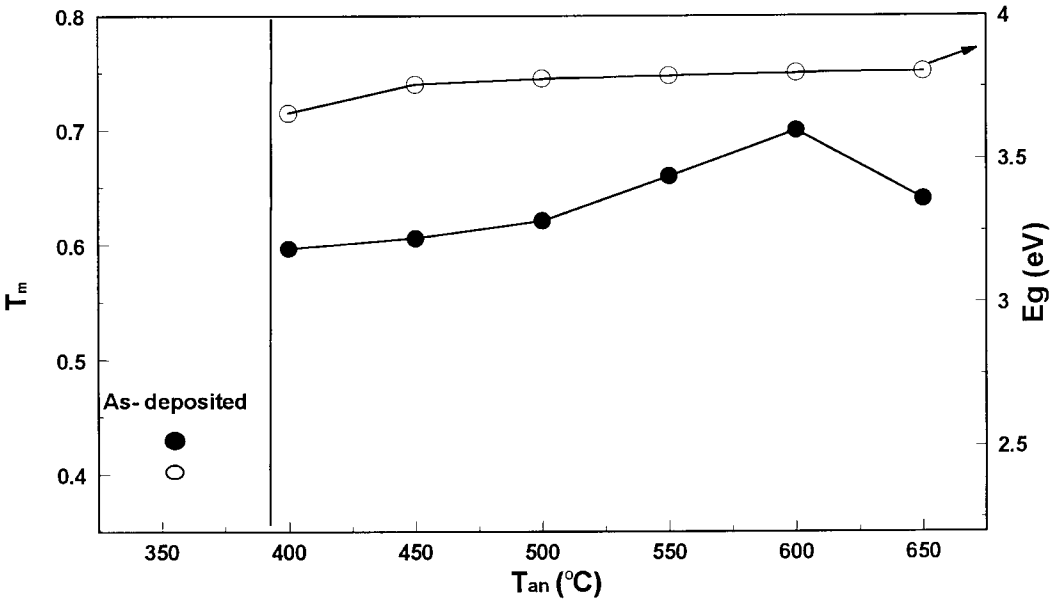

Fig. 4. Variations of the mean value T_m of the transmittance in the visible range and the width of optical gap with annealing temperatures, $t_{an} = 15$ min and $t = 100$ nm.

In order to predict the selective properties of transparent-conductive coatings from the fundamental optical and electrical properties, the factor of merit φ ($\varphi = T_m/\rho_{RT}$) can be employed [11,18]. As shown in Figure 5 and Table 2, φ, which has a maximum value of 2.04 ± 0.22 for film $\sim$ 100 nm thick annealed at 550 °C for 15 min (Fig. 5), can be improved with increasing either the film thickness and/or the time of annealing at 550 °C (Tab. 2).

4 Structural analysis

As shown in Figure 6, the X-ray diffractograms of the as-deposited Sb:SnO_2 film reveals some peaks with small intensities corresponding to the crystalline phases of SnO_2, SnO, Sb_2O_5, Sb_2O_3 and may be SbO_2 oxides, which are embedded in an amorphous matrix. Therefore, the as-deposited film can be considered as nearly amorphous. Almost similar structure could be observed for the film annealed at 400 °C. Whereas, as T_{an} is more elevated, the crystallinity increases mainly along (110), (101) and (211) directions of SnO_2 which have maximum values of intensity at $T_{an} = 550$ °C. Prolongation of t_{an} as well as the increase of thickness (t) lead to continuous increases in the film crystallinity along (110), (101) and (211) of SnO_2 too. Besides, these peaks characterizing SnO_2 seem to shift to lower values of 2θ with increasing T_{an}, t_{an} or t indicating an increase of the lattice constant [7] with these factors. Figure 7 and Table 2 confirm this increase of the lattice constant a (Å), which was deduced using the SnO_2 (110) peak, where $a = d(h^2 + k^2 + l^2)^{1/2}$, d is the distance of net planes and h, k and l are Miller indices, with T_{an} and t_{an} & t respectively. This suggests that some of the Sn^{4+} ions in the SnO_2 lattice are replaced by Sb^{3+} ions having larger ionic radii [20,23]. On the other hand, peaks (001), (101) & (102) corresponding to SnO oxide, seem to increase slightly with T_{an}, t_{an} and/or t. Furthermore, although slight nonsequential changes can be observed in peak-intensity of the existed phases of Sb-oxides, an additional peak corresponding to Sb_2O_5 appears for thicker films and longer annealing times.

Figure 8 shows the scanning electron micrographs of Sb:SnO_2 films with different thicknesses and conditions of annealing. It is clear that the surface of as-deposited film

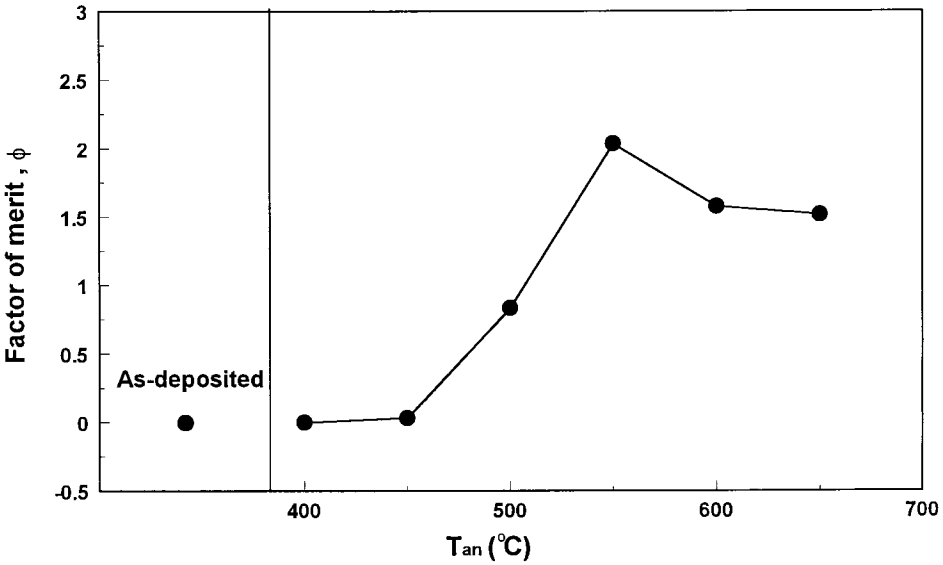

Fig. 5. Annealing temperature dependance of the factor of merit ϕ for Sb:SnO_2 films, t_{an} = 15 min & t = 100 nm.

Table 2. Effect of annealing time and thickness on some electrical and optical parameters of Sb:$Sn0_2$ films. (T_{an} = 550 °C).

Parameter		t(nm) = 100				t_{an}(min) = 180	
	As-deposited	t_{an} (min) = 15	90	120	180	t (nm) = 150	200
ρ_{RT} (Ωcm)	(4.06-4.22) $\times 10^6$	0.24-0.36	0.27-0.33	0.13-0.16	0.06-0.07	0.05-0.06	0.04-0.05
T_m %	43	66	86	86.5	86	78	75.6
φ	(1.02-1.06) $\times$ 10^{-7}	1.83-2.28	2.61-3.19	5.41-6.65	12.29-14.33	13-15.6	15.1-18.9
$-S(\mu V/K)$	—	0.70	1.50	1.62	1.80	1.92	2.22
a, Å	4.655	4.733	—	—	4.758	4.780	4.711
$\bar{n}$	1.98	2.16	2.15	2.19	2.27	2.18	2.22

is smooth and contains very fine grains. This confirms the nearly glassy nature of the film structure. Increasing the annealing temperature, annealing time and/or film thickness leads to the growth of disconnected grains, which can be correlated to the grown phases identified by the X-ray diffractograms in Figure 6. These disconnected grains seem to be embedded in a large glassy matrix as it is indicated by the smoothness of the film surface.

5 Discussion

As shown in Figure 1, the temperature range of hopping conduction, which is excessively wide, extends to temperatures over RT. The increase of annealing temperature leads to more extension of this hopping range as well as to a decrease in the high temperature activation energy (see Tab. 1). This behaviour of electrical conduction with increasing T_{an} may be attributed to the effect of glassy matrix contained in Sb:SnO_2 films and retained even for elevated values of T_{an} (see Figs. 6 & 8). These results may support the suggestion of Carroll and Slack [20] that Sb acts as a glass network former in the amorphous SnO_2. Besides, Hsu and Ghandhi [35] have reported that the introduction of glass former into SnO_2 greatly reduces the mobility of the reactant species on the surface making a tendency for the formation of amorphous solid. Moreover, the slight increase observed for SnO with T_{an} as shown in Figure 6 leads to the increase of disorder in SnO_2 films [44]. Otherwise, the large values of the optical band gap width E_g (Fig. 4) with respect to those corresponding to the high temperature activation energy ΔE (Tab. 1), which is consistent with many works on glassy chalcogenides and oxides (see for example Ref. [36]), can be accounted for the effect of Sb:SnO_2 glassy matrix too. This difference in E_g and ΔE values has been explained by that the electronic activation is not across the whole mobility gap but is possible from one or more trapping levels to the conduction band or from bonding states to a trapping level [36].

Results of Seebeck coefficient with annealing temperature (Fig. 2), annealing time and film thickness (Tab. 2) may lead to the following conclusions; (i) The negative sign of thermopower observed for Sb:SnO_2 films means that the major contribution results from electrons. These electrons are mainly produced due to the substitution of Sb^{5+} in the Sn^{4+} sites of SnO_2, which creates donor levels near the conduction band edge. Besides, the formation of SnO on the expense of SnO_2 content (see Fig. 6) leads to the increase of disorder and acts as donor [7,37]. (ii) The small values of S are consistent with the variable-range hopping model. On the other hand, they suggest that two

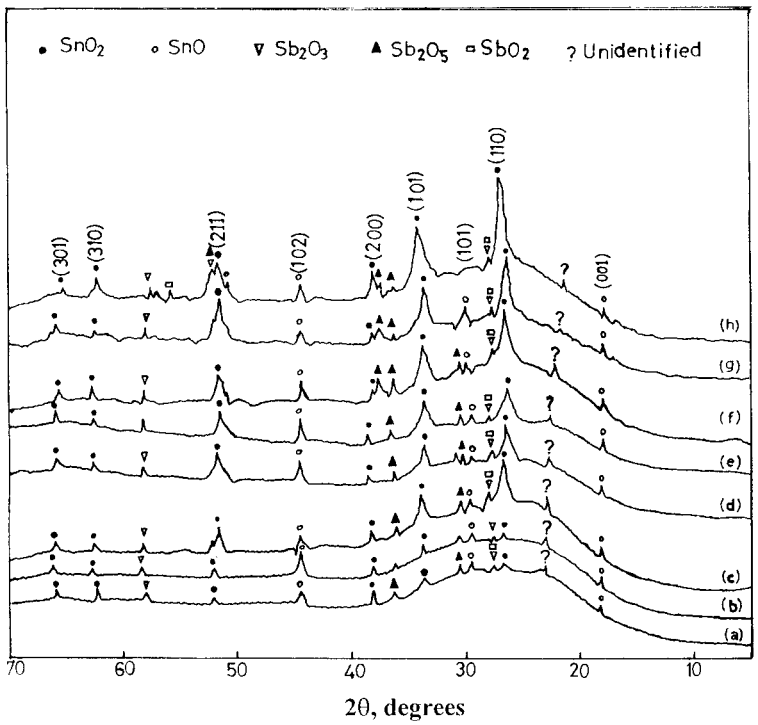

Fig. 6. X-ray diffraction patterns of Sb:SnO_2 films with Sb/Sn = 0.10. a-for as-deposited film (t = 100 nm); b, c, d and e after annealing at 400, 550 and 600 °C respectively (t_{an} = 15 min, t = 100 nm); f–after annealing for 180 min (T_{an} = 550 °C, t = 100 nm) and g, h–for films with thickness of 150 and 200 nm respectively (T_{an} = 550 °C, t_{an} = 180 min).

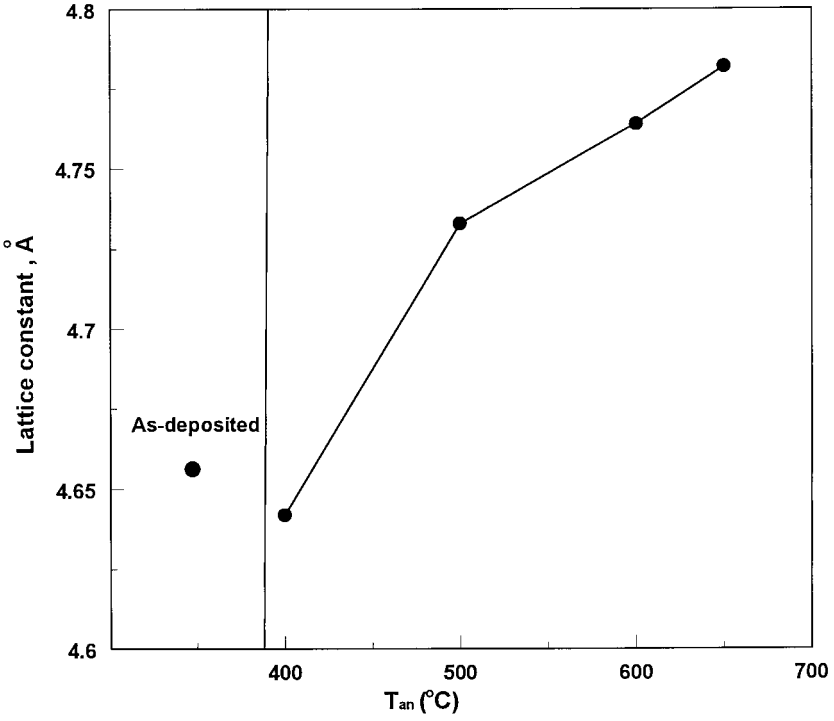

Fig. 7. Variation of the lattice constant a (Å) with annealing temperature.

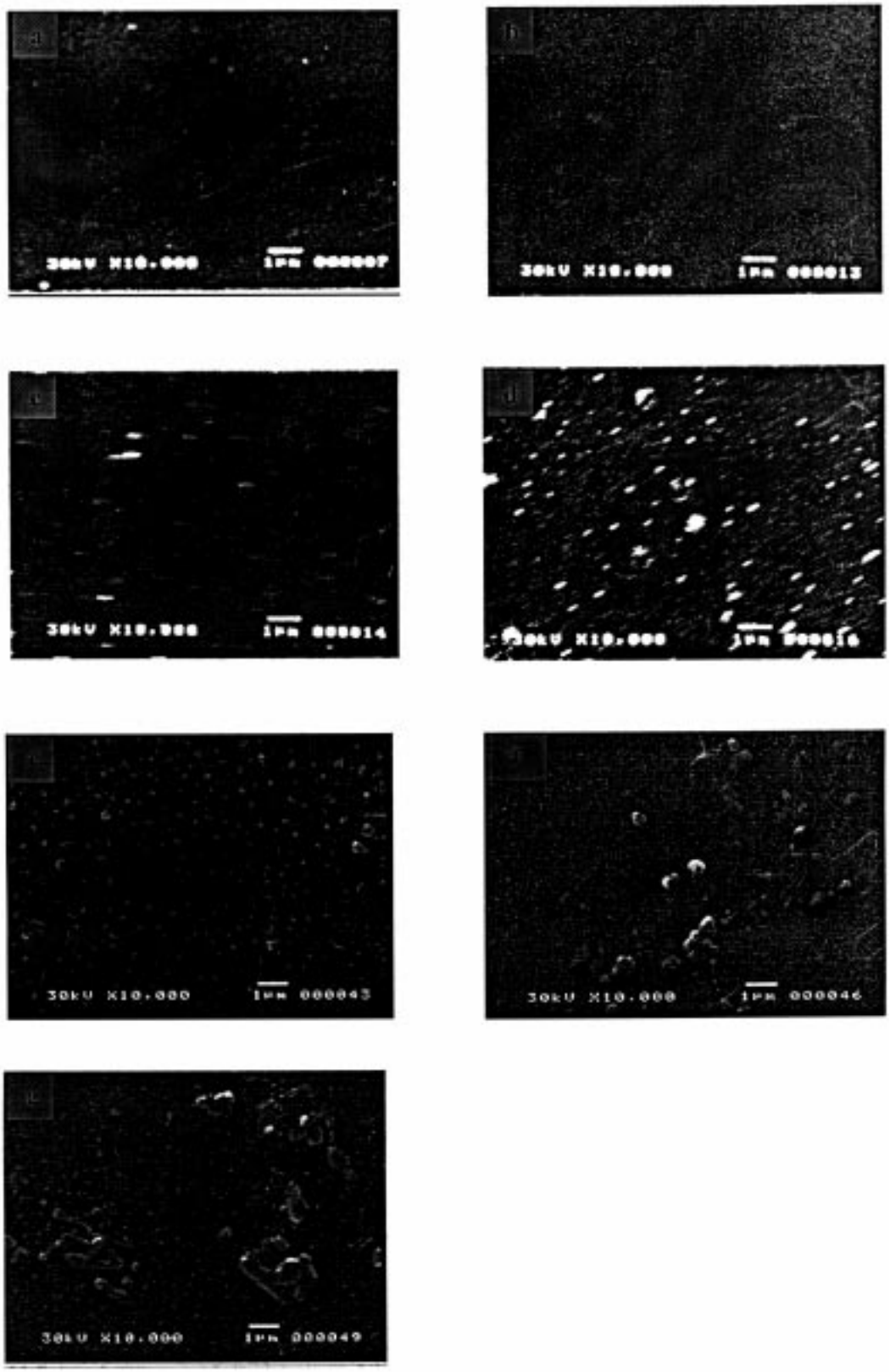

Fig. 8. Scanning electron microphags of Sb:SnO_2 films with Sb/Sn = 0.1; a- for as-deposited (t = 100 nm); b, c, d–after annealing at 400, 550 and 600 °C respectively (t_{an} = 15 min, t = 100 nm); e–after annealing for 180 min (T_{an} = 550 °C, t = 100 nm) and f, g-for films with thickness of 150 and 200 nm respectively (T_{an} = 550 °C, t_{an} = 180 min).

types of unlike charges can participate in the conduction (*i.e.* mixed conduction). In fact, the formation of Sb_2O_3 with T_{an} by substitution of trivalent Sb ions in Sn^{4+} sites of SnO_2 lattice as mentioned before, which acts as an acceptor, gives rise to the creation of opposite charges. (iii) Due to the compensation effect performed by these unlike charges, S is expected to decrease with T_{an}. (iv) However, the observed increase of S with either the annealing time at 550 °C or film thickness of annealed films at 550 °C for 180 min may be attributed to the increase of both the mobility and concentration of electrons due to the increase of crystallinity of SnO_2 phases and/or the appearance of additional Sb_2O_5 phases respectively, see Figure 6.

As shown in Table 1, values of the density of localized states $N(E_f)$ are unreasonably high. Similar results have been reported for other works [38] and attributed to the large number of simplifying assumptions introduced to Mott's relation, which leads to uncertainties in the estimated values of Mott's parameters. On the other hand, these high values of $N(E_f)$ may be acceptable since SnO created on the expense of SnO_2 results in additional states at E_f [19,37]. Besides, it has been formerly proved [9] that, the energy of states introduced by the Sb-O bonds lie at energy levels, which are outside the band region of the SnO_2, since the energy of Sb-O bonds are larger than that of Sn-O [39]. This leads to that the Fermi level lies more deeply within the band gap and consequently, Sb that acts as a glass former [30] does not participate in the creation of carriers [9]. Thus, the crystallinity improvement, especially, along some SnO_2 phases may be responsible for the observed elimination of the localized states participating in the hopping conduction.

As shown in Figure 2, the as-deposited Sb:SnO_2 film shows high value of the room temperature resistivity ($\rho_{RT} = 4.23 \times 10^6$ Ωcm), which is attributed to the lower degree of crystallinity in the film, see Figure 6. Annealing at 400 °C for 15 min results in a significant decrease in the film's resistivity to be 2.2 $\times 10^2$ Ωcm. Minimum value of ρ_{RT}, which is 0.247 Ωcm, can be observed for the film annealed at 550 °C. This means that, annealing at 550 °C for 15 min leads to a drop in film's resistivity by about seven orders. This decrease in ρ_{RT} with T_{an} could be attributed to the improvements of the film structure ordering and mobility with annealing. For more clarification, evaluations of the room temperature concentration N and mobility μ of the electrons participating in conduction within a range KT of the Fermi energy using that $N = 2KT\,N(E_f)$ and $\mu = 1/(Ne\rho_{RT})$ have been performed. Results of N and μ, which are recorded in Table 1, show that the elevation of T_{an} leads to a decrease in the concentration of electrons and enhancing their mobility. In general, the mobility μ is a function of both μ_v and μ_n, which are related to the grain boundary potential and the impurity concentration respectively, as follows: $1/\mu = 1/\mu_v + 1/\mu_n$. Assuming that the concentration of Sb atoms, which represents the impurity atoms in the SnO_2 lattice, is constant, the contribution of μ_n to the carrier mobility is assumed to be constant. However, the increase of grain size causes a decrease in the density of grain boundaries, which act as traps for free carriers and barriers for carrier transport [40]. According to [41–43], it can be assumed that the observed increase in free carrier mobility and consequently the decrease in ρ_{RT} with annealing temperature is due to an improved crystallinity of Sb:SnO_2 films, especially along (110), (101) and (211) SnO_2 peaks as shown in Figure 6. Besides, the annealing at $T_{an} > 550$ °C is associated with a slight increase in the resistivity, Figure 2. Kojima *et al.* [8] have reported similar results for Sb:SnO_2 films prepared by spray pyrolysis and attributed them to the antimony accumulation at the surface for films annealed at temperatures higher than 600 °C . Besides it has been suggested [27,28] that heat treatment of Sb:SnO_2 at temperatures over 700 °C causes the antimony to migrate rapidly to the surface. Then, the results given in Figure 2 may be accounted for. However, the continuous decrease of ρ_{RT} with annealing time ($T_{an} = 550$ °C) and/or film thickness can be predicted since both the concentration and mobility of carriers with these factors have generally increased as mentioned before .

As shown in Figure 4 and Table 2, the heat treatment of Sb-doped SnO_2 films improves their transparency. Values of the film transmittance (T_m) before and after annealing at 400 °C for 15 min are 0.43 and ∼ 0.60 respectively. It exceeds 0.86 for film annealed at 550 °C for 120 min. In the same time, as shown in Figure 6, the heat treatment improves the degree of film crystallinity. In contrast, Kojima *et al.* [9] have proved that the amorphous Sb-Sn-O films prepared by spray pyrolysis are transparent while those having crystalline structure are opaque. In fact, the opacity of the crystalline films arises from the high energy absorption during the electron exchange among Sb^{3+} and Sb^{5+} substituted on Sn site in SnO_2 lattice. On the other hand, this process can not take place in amorphous Sb-Sn-O films due to the asymmetrical atmosphere around Sb^{3+} and Sb^{5+} ions caused by the difference in their coordination as a result of the oxygen deficiency. Moreover, it has been concluded [7] that, the formation of SnO oxide on the expense of SnO_2 content, which is required by the local charge neutrality, confirms the deficiency in oxygen content in Sb:SnO_2 films. For the present films, the X-ray diffractograms shown in Figure 6, revealed mainly the phases (001), (101) and (102) of SnO oxide. This means that, the coordination of trivalent and pentavalent ions of antimony corresponding to Sb_2O_3 and Sb_2O_5 oxides respectively, which could be recognized and slightly increased in peak intensity as shown in Figure 6, may be different. Therefore, accordingly [21, 22,44], it is difficult for electron transfer to take place and consequently the transmittance of the present films increases even with simultaneous increase in the degree of crystallinity due to annealing. Otherwise, the decrease in T_m observed with the film thickness, see Table 2, might be attributed to the improvement of the process of charge transfer between the two oxidation Sb^{3+} and Sb^{5+} states of antimony with thickness.

Finally, values of the refractive index $\bar{n}$ for Sb:SnO_2 films lie between 1.98 to 2.18 as shown in Table 1.

Regarding that the refractive index of undoped SnO_2 is approximately 1.9 [35], the present values for $\bar{n}$ may be acceptable since Sb atoms, which are considered as impurities in SnO_2 lattice, contribute to the increase of refractive index [45]. In addition, the observed increase in $\bar{n}$-values with both annealing time and film thickness as shown in Table 2, may be attributed to the increase of film compactness associated with the increase of film crystallinity with these factors.

6 Conclusions

Structural features characterizing Sb:SnO_2 films elaborated by the present method have found to be stimulated by annealing and/or film thickness changes and collaborated to give as a result a transparent conductive film. After annealing at 550 °C for 180 min and raising the film thickness to 200 nm, the room temperature resistivity has dropped by about eight orders of magnitude to be 4.4×10^{-2} Ωcm and the average transmittance in the visible range has improved to be around 80%. In addition, the observed continuous increase of the factor of merit with annealing and/or film thickness suggests that further improvements of σ and T_m may be achieved with more increase of annealing time (at 550 °C) and/or film thickness. Furthermore, the present elaborating method may be of economic usefulness. Sintering process is an inexpensive method for producing lumps of powdered materials and the deposition by electron beam provides economical and efficient usage of evaporant. Thus, the Sb:SnO_2 film elaborated in the same present argument may be considered as a promising material for many technical applications.

References

1. A. Messad , J. Bruneaux, H. Cachet, M. Froment, J. Mat. Sci. **29**, 5095 (1994).
2. R. Bellingham, W.A. Phillips, C.J. Adkins, J. Mat. Sci. **11**, 263 (1992).
3. R.N. Ghosthagore, J. Electrochem. Soc. **125**, 110 (1978).
4. T. Maruyama, K. Tabata, J. Appl. Phys. **68**, 4282 (1990).
5. A. Smith, J.M. Laurent, D.S. Smith, J.P. Bonnent, R. Rodriguez-Clemente, Thin Solid Films **266**, 20 (1995).
6. G. Gordillo, L.C. Moreno, W. De la Cruz, P. Teheran, Thin Solid Films **252**, 61 (1994).
7. M. Kojima, H. Kato, M. Gatto, Philos. Mag. B **68**, 215 (1993).
8. M. Kojima, H. Kato, M. Gatto, Philos. Mag. B **73**, 289 (1996).
9. M. Kojima, H. Kato, M. Gatto, Philos. Mag. B **73**, 277 (1996).
10. M. Kojima, H. Kato, M. Gatto, J. Non-Cryst. Solids **218**, 230 (1997).
11. C. Terrier, J.P. Chatelon, J.A. Roger, Thin Solid Films **295**, 95 (1997).
12. A. Tsunashima, H. Yoshimiza, K. Kodana, S. Shimada, T. Matsushita, J. Mat. Sci. **21**, 2731 (1986).
13. B. Stjenna, C.G. Granqvist, Solar Energy Mat. **20**, 225 (1990).
14. E. Leja, T. Pizarkiewicz, A. Kolodziej, Thin Solid Films **67**, 45 (1980).
15. H. Demiryont, N. Tezey, Thin Solid Films **101**, 345 (1983).
16. A.K. Saxena, R. Thangaraj, S.P. Single, P. Agnihorti, Thin Solid Films **131**, 121 (1985).
17. M.B. Gottlieb, R. Koropecki, R. Arce, R. Crisalle, J. Ferron , Thin Solid Films **199**, 13 (1991).
18. G. Haacke, Appl. Phys. Lett. **28**, 622 (1976).
19. E.Kh. Shokr, M.M. Wakkad, H.A. Abd EL-Ghanny, H.M. Ali, J. Phys. Chem. Solids (to be published).
20. A.F. Carroll, L.H. Slack, J. Electrochem. Soc. **123**, 1889 (1976).
21. M.B. Robin, P. Day, Adv. Inorg. Chem. Radiochem. **10**, 247 (1967).
22. A.C. Skapski, D. Rogers, Chem. Commun., 611 (1965).
23. R.D. Shannon, Acta crystallogr. A **32**, 751 (1976).
24. F. Decker, J. Melsheimer, H. Gerischer, Isr. J. Chem. **22**, 195 (1982).
25. W. Badawy, F. Decker, K. Doblhofer, Solar Energy Mat. **8**, 363(1983).
26. W. Badawy, K. Doblhofer, I. Eiselt, H. Gerischer, S. Krause, J. Melsheimer, Electrochem. Acta **29**, 1617 (1984).
27. Y. Boudeville, F. Figueras, M. Forissier, J.L. Prte Faix, J.C. Vedrine, J. Catal. **58**, 52 (1979).
28. G.B. Hoflund, D.F. Cox, G.L. Woodson, H.A. Laitinen, Thin Solid Films **78**, 357 (1981).
29. J.C. Manifacier, J. Gasiot, J.P. Fillard, J. Phys. E **9**, 1002 (1976).
30. T.S. Moss, *Optical properties of semiconductors* (Academic Press , New York, 1959), p. 40.
31. E.Kh. Shokr, J. Phys. Chem. Solids **53**, 1215 (1992).
32. N.F. Mott, Philos. Mag. **19**, 835 (1969).
33. H. Fritsche, in *Amorphous and Liquid Semiconductors*, edited by J. Tauc (Plenum, London, 1974), p. 221.
34. D. Jousse, Phys. Rev. B **31**, 5335 (1985).
35. Yar-Sun Hsu, K. Sorab Ghandi II, J. Electrochem. Soc. Solid Stat Sci. Technol. **127**, 1592 (1980).
36. M.A. Hassan, C.A. Hogarth, J. Mat. Sci. **23**, 2500 (1988).
37. G.A. Khan, C.A. Hogarth, J. Mat. Sci. **25**, 3002 (1990).
38. R.M. Mehra, R. Kumar, P.C. Mathur, Thin Solid Films **170**, 15 (1989).
39. W.D. Kingery, H.K. Bowen, D.R. Uhlmann, *Introduction to Ceramics* (Wiley, New York, 1976), p. 99.
40. K.H. Heckner, Phys. D. Halbleiteroberfläche **17**, 197 (1986).
41. Y. Sadaoka, T.A. Jones, W. Göpel, S. Kimura, N. Honda, J. Mater. Sci. **25**, 2632 (1990).
42. E. Bertran, J.L. Morenza, M. Verela, Thin Solid Films **129**, 103 (1985).
43. L.I. Maissel, R. Glang, *Handbook of Thin Film Technology* (McGraw-Hill, New York, 1970).
44. D. Rogers, A.C. Skapski, Proc. Chem. Soc., 400 (1964).
45. E. Bertran, A. Lousa, M. Varela, M.V. Cuenca, J.L. Morenza, Solar Energy Mat. **17**, 55 (1988).